The Three-Dimensional Nature of Interaction Regions: Pioneer, Voyager, and Ulysses from 1 to 5 AU: Solar Cycle Variations

J. Américo González-Esparza and Edward J. Smith

Jet I'repulsion Laboratory, California Institute of Technology, Pasadena

Received . . . _____; accepted _____

Short title: GONZÁLEZ-ESPARZA ANI) SMITH: SOLAR CYCLE AND INTERACTION REGIONS

Abstract. We investigated diverse aspects of the interaction regions detected by four spacecraft that traveled from Earth to Jupiter at different phases of the solar cycle: Pioneer 11 (declining phase of cycle 20); Voyagers 1 and 2 (ascending phase of cycle 21); and Ulysses (just after solar maximum 22). From the analysis of 38 stream interfaces we found that the interaction regions detected by the three missions have different geometries. Some of these results might be associated with solar cycle variations such as the low latitudinal inclination of the interaction regions detected by Ulysses and the latitudinal tilts of the interaction regions detected by Pioneer 11. Other results, such as the deviations with respect to the Parker spiral orientation, seem to be related to persisting changes in the characteristics of the fast and slow solar winds causing the interaction regions, We studied the properties of the solar wind streams associated with 75 interaction regions. The bulk speed distributions of the fast ant] slow streams were different in the three missions. We fount] that the pressure ratios (dynamic, thermal, magnetic) between fast and slow winds vary continuously. In fact, in about half of the interaction regions the dynamic pressure of the slow stream was higher than the dynamic pressure of the fast stream. This implies that, contrary to the usual assumption, in many interaction regions the slow stream transfers momentum to the fast stream. The pressure ratios between a fast and a slow stream causing an interaction region can vary at different locations. This would deform the spiral configuration of the interaction region.

1. Introduction: Stream Interfaces

The distinct boundary separating fast and slow solar wind flows, that is characterized by an abrupt drop in density, a similar increase in temperature, and it is associated with a high pressure region is called stream interface [*Burlaga*, 19'74]. *Siscoe et al.* [1969] predicted east-west and north-south deflections of solar wind velocity close to stream interfaces. These deflections result from the high thermal and magnetic pressures associated with the interface. In the interface reference system: the fast stream comes from the west and the slow stream comes from the east. so the pressure acts to deflect the fast stream to the east and the slow stream to the west causing a strong shear flow (see e.g.. Figure 1 in *Siscoe et al.* [1969], Figure 2 in *Pizzo* [1991]).

Gosling *et* al. [1976] studied 23 interfaces detected by 1111'6, 7 and 8 at 1 AU between 1971 and 1974. They produced a superposed epoch analysis to emphasis the overall structure of the stream interfaces and reported that: (1) the behavior of protons. electrons and alpha particles across the interface suggests that it separates plasma of distinctly different origins: (2) there is a strong shear flow at the interface; (3) the magnetic field strength maximizes near the interface and is roughly constant across it; (4) although their observations were made during the descending phase of solar cycle 20, the interfaces did not generally recur from one solar rotation to the next.

Figure 1 shows an example of an interaction region detected by Pioneer 11 at 4.3 AU. At the bottom fast solar wind (V_r > 70(I km/s) overtakes slow wine] ($V_r \leq 400$ km/s) causing an interaction region. The stream interface separates the two

compressed flows and is recognized by: the solar wind shear flow (top panel); the abrupt drop in density and increase in proton temperature (mid-panel); and the high magnetic field magnitude (bottom panel).

In this paper we explore other aspects of stream interfaces. Our study is based on observations in a different heliocentric range (1 to 5 AU) from the previous studies where interfaces and interaction regions are well formed. We combine observations by four different spacecraft that covered the same heliocentric range at different phases of the solar cycle. We report findings on: (1) the three-dimensional geometry of t he stream interface; (2) its variation with the solar cycle; and (3) ever-presented differences in the physical properties of the fast and slow solar wind streams causing the interaction regions.

1.1. Ulysses Observations of Interaction Regions at Mid-Latitudes

Ulysses observations have increased interest in the three-dimensional heliosphere. One of the main results obtained by Ulysses after the Jupiter flyby was tile absence. from about 28° to 38° south latitude, of interplanetary shocks leading interaction regions and the continuous presence of reverse shocks trailing these interaction regions [*Gosling et al., 1993; Balogh et al.,* 1994; *Pizzo and* Gosling, 1934; *González-Esparza et al.,* 1996]. On the basis of the strong latitudinal shear flows of solar wind velocity inside these interaction regions and the predictions by the three-dimensional model of corotating flows by *Pizzo* [1982, 1991, 1994], *Gosling et al.* [1993] suggested that this phenomenon detected by Ulysses during the descending phase of solar cycle 22 could be explained

if the interaction regions were tilted with respect to the solar rotation axis. This tilt geometry causes the front of the interaction region to evolve stronger at low latitudes (c1osc to the ecliptic plane) whilst the trailing edge evolves stronger at higher latitudes (see, e.g., Figure 3 in *Pizzo* [1994], Figures 3 and 4 in *Pizzo and Gosling* [1994]) and produces a strong latitudinal shear flow inside the interaction region.

The three-dimellsional model of corotating flows by *Pizzo* [1 982,1991, 1 994] shows that two opposite tilted interaction regions are formed if: (1) the solar magnetic field can be approximated to a dipole, and (2) there is a tilt angle between the solar rotation and magnetic axis (see e.g., Figure 2 in *Pizzo* [1994]), These conditions are only a good approximation during the descending phase of tile solar cycle [*Zhao and Hundhausen*, 1981; *Mihalov*, 1990] which coincides with Ulysses' trajectory after the Jupiter flyby. In order to corroborate the predictions of the model, the normals of the corotating shocks detected by Ulysses after the Jupiter flyby in 1992 and 1993 (from 6° to 38 ° south heliolatitudes) had been studied, *Burton et al.* [1996] used high time resolution magnetic field data (1-2 seconds resolution) to apply a technique based on magnetic coplanarity to infer the shock normal directions. 'I'hey found a significant dispersion in the latitudinal orientation of the forward and reverse interplanetary shocks (Figure 6 in *Burton et al.* [1 996]). However, the distribution was qualitatively consistent with the 3-D model of corotating flows. *Riley et al.* [] 996] presented a detailed analysis of the corotating shocks based on solar wind plasma data. They used solar wind velocity data (4-8 minutes time resolution) to apply a technique based on velocity coplanarity to infer the shock normal directions. Note that to apply velocity coplanarity, it is assumed

necessarily that the shock is almost parallel ($\theta_{B_n} \approx 0°$) or perpendicular ($\theta_{B_n} \approx 90°$), however, the θ_{B_n} distribution of the corotating shocks detected by Ulysses after the Jupiter flyby shows that most of these shocks were quasi-parallel or quasi-perpendicular ($20° < \theta_{B_n} < 70°$) (Figure 11 in *González-Esparza et al. [1996]).* The results found by *Riley et al.* [1996] show that on the whole, the forward corotating shocks were propagating equatoward and westward, while the reverse corotating shocks were stronger and propagating poleward and eastward as expected.

The variations in the pattern of solar wind stream streams [Gosling *et al.*, 1976; *González-Esparza and Smith,* 1996] and the evolution of coronal holes [*Hundhausen et* al., 1981] and neutral sheet [*Hoeksema,* 1986] through the solar sunspot cycle suggest that interaction regions should have a different geometry and characteristics at different phases of the cycle. In this study we investigate the orientation of the interaction regions, however, instead of applying Rankine-Hugoniot relations to infer the normals of the shocks leading and trailing the interaction regions, we will use a different approach. We will analyze the shear flows of solar wind velocity at tile interface based on a variation of the principal axis analysis technique. The convenience and limitations of this technique are discussed in section 2.1.

1.2. Solar Cycle Variations: Pioneer, Voyager, and Ulysses from 1 to 5 AU

González-Esparza and Smith [1996] (hereafter paper 1) unified and compared the in-ecliptic observations of large-scale solar wine] dynamics by Pioneers 10 and 11, Voyagers 1 and 2, and Ulysses from 1 to 5 AU. The three missions covered the same

heliocentric range at different phases of the. solar cycle: Pioneer (descending phase cycle 20); Voyager (ascending phase cycle 21); and Ulysses (post-maximum cycle 22) (see Figure 1 in paper 1). Continual variations in the solar wind dynamics were detected by the three missions: changes in the pattern of solar wine] streams produce persisting transitions from periods dominated by interaction regions to periods dominated by transient events and viceversa. T 'here were also differences and similarities between the shock population and interaction regions detected by the three missions. Some interesting questions arise from the previous study: how different are the interaction regions detected by Pioneer, Voyager, and Ulysses? How do the continual changes of solar wind streams affect the properties of the interaction regions? How do the characteristics and orientation of the interaction regions change with the solar cycle?

2. Geometry of Stream Interfaces

In paper 1 we identified all the interaction regions detected by the five spacecraft from 1 to 5 AU and we plotted them in maps of large-scale features (Figures 3-7 in paper 1). As expected during the descending phase of the cycle, Pioneer 11 detected a very regular pattern of solar wind streams, magnetic sectors and corotating interaction regions. On the other hand, the other spacecraft observed variable patterns of solar wind dynamics. By visual inspection we noted that the solar wind plasma and magnetic field profiles of the interaction regions detected by the three missions were very different. In this paper we will compare Pioneer 11, Voyagers 1 and 2, and Ulysses observations. We did not include Pioneer 10 observations because we consider that the large number

(50) and regularity of the interaction regions detected by Pioneer 11 were a very good sample of these events at the descending phase of the cycle. We used solar wind plasma data (1 hour averages) from the NSSDC which is readily available for the four spacecraft. This temporal resolution is adequate to study the large-scale geometry, not the local structure, if the shear flow is well-defined and the interface can be approximated by a tangential discontinuity. Previous studies had used this temporal resolution to study other large-scale properties of stream interfaces [*Siscoe et al.*, 1972; *Gosling et al.*, 1976].

2.1. Maximum Variance Analysis: Stream Interface Reference System

Siscoe et al. [1972] analyzed the shear flows of solar wind velocity at 6 streams interfaces detected by Pioneer 6 at 1 AU. Under the assumption that the solar wind velocity along the interface normal direction was approximately constant (i. e., there was not net flow through the interface), they applied the principal axis analysis to tile solar wind velocity data surrounding the interface and identified the minimum variance direction (the eigenvector associated with the minimum eigenvalue) as the interface normal. They neglected the effects associated with the latitudinal flows and reported that the interfaces were closely oriented along the Parker spiral,

There is a problem in applying tile minimum variance technique to infer tile interface normal direction. Although, in many *cases*, the maximum variance direction is well-defined along the shear flow velocity parallel to the interface plane, the minimum variance direction is ill-defined (any direction orthogonal to the maximum variance direction, in theory, has a zero variance). In order to infer a more accurate result and

to solve this 'velocity coplanarity problem', it is necessary to modify the technique by transforming to the 'interface reference system'. This method can be summarized as follows: (1) We select an interval of solar wind plasma data of a few hours before and after the interface of at least 8 hours (8 data points) which contains a well-defined discontinuity and a strong shear flow. (2) We apply the principal axis analysis to the solar wind velocity to obtain the three eigenvectors $(\hat{\mathbf{n}}_{max}, \hat{\mathbf{n}}_{int}, \hat{\mathbf{n}}_{min})$. (3) We transform the interval of velocity data $(\vec{V})$ to the principal axis reference system to obtain averages values along the three eigenvectors $(\overline{V_{max}}, \overline{V_{int}}, \overline{V_{min}})$. (4) We transform to tile 'stream interface reference system' rotating the principal axis reference system along the maximum variance direction (1.0.0) an angle $\alpha = \arctan(V_{int} / V_{min})$. The three normals vectors of the interface reference system are: $\hat{\mathbf{n}}_{si_{t1}}$ along the maximum variance direction, parallel to the interface plane; $\hat{\mathbf{n}}_{si_{t2}}$ also contained in the interface plane and orthogonal to $\hat{\mathbf{n}}_{si_{t1}}$ (along this component the solar wind velocity has a an average value about zero); and the interface normal direction $\hat{\mathbf{n}}_{si_n}$ along which the solar wind velocity has an average value different from zero.

Not all the interaction regions contain a well-defined interface. In fact, we could not analyze most of the events. We only applied the technique to those events with a well-defined discontinuity in plasma parameters and a strong shear flow. We did not analyze interaction regions with data gaps or those containing large amplitude temporal variations. To make sure that the maximum variance direction was well-defined, we used as criteria that the maximum eigenvalue was at least 5 times larger than the other two, and we varied the length of the interval to check that the result was stable.

2,2. Results: Orientations of Interfaces

Voyager 1 detected 17 interaction regions from which we were able to analyze only 4 of them. Voyager 2 detected 13 interaction regions from which we were able to analyze 5 of them. Ulysses detected 17 interaction regions from which were able to analyze 9 of them. Pioneer 11 detected 50 interaction regions from which we were able to analyze 20 of them. Figure 2 shows interface latitudinal inclinations θ_{si} against heliocentric distance as deduced from the four spacecraft,. θ_{si} would be equivalent to the latitudinal tilt of the interaction region where: $\theta_{si} > 0°$ implies that the front of the interaction region was pointing northern. $\theta_{si} \approx 0°$ implies that the interaction region was not tilted, and $\theta_{si} < 0°$ implies that the front of the interaction region was pointing southern. Voyagers (top panels) and Pioneer 11 (bottom panel) results show variable θ_{si}'s with many interfaces with significant latitudinal tilts. However, Ulysses results show small θ_{si} suggesting that its interaction regions were closely perpendicular to the ecliptic plane. We should keep in mind that the four spacecraft detected unstable patterns of solar wind streams (Figures 2 and 8 in paper 1). The variances in θ_{si} detected by Voyagers and Pioneer 11 arc more likely associated with these changes of solar wind streams than with heliocentric effects (Ulysses' out-of-ecliptic results show similar fluctuations in θ_{si} (Figure 5 in *Riley et al. [1996])).*

Figure 3 shows the θ_{si} distribution histograms as detected by the three missions. There is a clear difference in the latitudinal tilts of the interaction regions detected by Ulysses and the ones detected by Voyagers and Pioneer 11. Ninety percent of the

interfaces detected by Ulysses had an absolute latitudinal tilt $|\theta_{si}|$ lesser than 5°; whilst fifty-five percent of Voyager and Pioneer 11 interfaces had a $|\theta_{si}|$ larger than 10°. This result might be associated with the solar cycle. Ulysses observations were made just after the maximum of cycle 22, when we do not expect polar coronal holes but small holes at mid-latitudes [*Hundhausen et al.*, 1981]. Interaction regions caused by fast streams from equatorial coronal holes are not expected to have significant tilts close to the ecliptic (see, e.g., Figure 3 in *Siscoe* [1976]; Figure 14a in *Pizzo* [1982]). On the other hand, pioneer 11 interaction regions are expected to have inclinations produced by the tilted solar geometry commented on in section 1.1.

Do the interfaces follow a Parker spiral? To answer this question we compared the ill-ecliptic longitudinal orientation of the stream interface ϕ_{si} with its corresponding in-ecliptic Parker spiral angle ϕ_{Ps}:

$$\phi_{Ps}(si) = \arctan\ (-\ \Omega_{\odot} \mathrm{R}(si)\ /\ \mathrm{V}_r(si))$$

(where $\Omega_{\odot}$ is the Sun's equatorial angular speed, $\mathrm{R}(si)$ is the heliocentric distance. and $\mathrm{V}_r(si)$ is the average solar wind radial velocity at the interface). Figure 4 shows the distribution histograms of the angle difference $\Delta\phi = \phi_{Ps} - \phi_{n_{si}}$, where $\Delta\phi \approx 0°$ means that the interface was aligned along the Parker spiral, $\Delta\phi < 0°$ means that the interface was more 'azimuthal' than the Parker spiral, and $\Delta\phi > 0°$ means that the interface was more 'radial' than the Parker spiral. Statistically, Voyagers and Ulysses results are very similar: in both cases about 67% (6 out of 9) of their interfaces were more azimuthal than the Parker spiral ($\Delta\phi \leq -10°$) and about 33% (3 out of 9) of their interfaces were

closely oriented along the Parker spiral ($|\Delta\phi| < 10°$). on the other hand, Pioneer 11 results show a more diverse distribution: 50% (10 out of 20) of its interfaces were closely oriented along the Parker spiral ($|\Delta\phi| < 1\,O°$); 20% (4 out of 20) of its interfaces were more azimuthal than the Parker spiral ($\Delta\phi \leq$ ---lO°); and 30% (6 out of 20) of its interfaces were more radial than the Parker spiral ($\Delta\phi \geq 10°$). 'he results from the three missions show some interfaces with significant deviations from the Parker spiral Some of these results can be associated with the variations of the physical properties of the solar wind streams causing interaction regions that we will discuss in section 3.1. We did not find a clear tendency in $\Delta\phi$ as a function of heliocentric distance in any of the four spacecraft. In the same way that we pointed out in Figure 3, the longitudinal variations $\Delta\phi$ seem to be a temporal effect more than a heliocentric evolution.

We could not analyze many interfaces due to large temporal fluctuations inside the interaction regions. These temporal fluctuations might be related to different causes: (1) the variability of the physical properties of the fast and the slow solar wind (section 3.1) might produce some interaction regions more unstable than others; (2) the expansion of the forward and reverse corotating shocks on the rarefaction zones trailing and leading the interaction regions; (3) the 'collision' of transient events (ejecta) and interaction regions.

3. Physical Parameters of Interaction Regions

Interaction regions arise when fast solar wind overtakes slow wind. The 'collision' between two different streams implies an interchange of momentum. In principle, there

should be a point where an equilibrium between the two streams is reached and the interface can be approximated to a tangential discontinuity. In that case, the Rankine-Hugoniot relation for the normal component of momentum establish that the sum of the dynamic pressure, plus the thermal pressure (in this case assuming that we can apply the state equation to the solar wind and that protons ancl electrons have broadly the same temperature). plus the magnetic pressure should be constant across the discontinuity:

$$\left[111_{p} N V_{n}^{2} + 2 N K T_{p} + B^{2}/(2\mu_{o}) \right] = 0 \qquad (1)$$

(where m_p is the proton mass. N is the proton density number, V_n is the solar wind velocity normal to the interface. K is the Boltzman's constant ($= 1.38 \times 10^{-23}$ J/ 'K), T_p is the proton temperature and B is the magnetic field magnitude). It is interesting to compare the orders of magnitude of the three parameters given typical solar wind values at 1 AU. Taking the proton density number as $N = 5\ cm^{-3}$ and the solar wind bulk velocity as $V_r = 450$ km s^{-1}, the solar wind dynamic pressure is about 1.69×10^{-9} Pa. With the same density number and the proton temperature as $T_p = 1.2 \times 10^5$ 'K, the solar wind thermal pressure is about 1.66×10^{-11} Pa. Finally, taking the magnetic field magnitude as $B = 5$ nT, the solar wind magnetic pressur$_e$ is about 9.95 x 10'12 Pa. The dynamic pressure is about 2 orders of magnitude larger than the thermal and magnetic pressures for typical parameters of the solar wind. The transference of dynamic pressures between fast and slow winds plays a predominant role in the formation and evolution of interaction regions.

We will compare the bulk speeds and pressures (dynamic, thermal, magnetic) of

the fast and slow streams causing interaction regions. We will show that the ratios of pressures (between fast and slow winds) vary continuously. This implies that the pattern of solar wind streams is, in general. more complex than the stable conditions assumed by the models of corotating flows and might explain why there are interaction regions with very different characteristics.

3.1. Variances in the Physical Parameters

To estimate the pressures ratios associated with every interaction region: (1) we selected an interval of solar wine] data of a few hours (4-7) just before and after the interaction region; (2) we averaged the bulk speed and pressures of the two streams; (3) we obtained the three pressure ratios, between fast and slow wind. associated with every interaction region: dynamic $r_{dyn.} = N_f V_f^2 / N_f V_f^2$, thermal $r_{ther.} = N_f T_{p_f} / N_s T_{p_s}$, and magnetic $r_{mag.} = B_f^2 / B_s^2$. Table 1 presents the averages of bulk speeds and pressure ratios as detected by the four spacecraft. The second column shows the number of interaction regions analyzed, where, contrary to the analysis of the stream interfaces, wc were able to study most of the events. The third column shows that the bulk speed average of the fast streams behind the interaction regions was much higher in Pioneer] 1 and Ulysses than in Voyagers 1 and 2. The fourth column shows that the bulk speed average of the s1ow streams preceding the interaction regions was much higher in Ulysses and lower in Voyager 2, These results are related to the changes in the distribution of solar wind bulk speeds through the solar cycle that was discussed in paper 1. The fifth column presents the average and standard deviation of the ratios of dynamic

pressures $r_{dyn.}$. Note the large standard deviation associated with every average. In many interaction regions, due to the difference in proton density, the dynamic pressure of the slow stream was higher than the dynamic pressure of the fast stream. Ulysses and Pioneer 11 $\overline{r_{dyn.}}$ are very similar, but Voyager 1 and 2 differ significantly. In paper 1 we pointed out that the observations of large-scale dynamics by the two Voyagers vary in many aspects (e.g., on the average on the whole trajectory (1 to 5 AU) Voyager 1 detected about 1.2 interaction regions per solar rotation (27 clays) while Voyager 2 detected about 0.8 interaction regions per solar rotation). Voyager 2 observed lowest average values of solar wind bulk speeds associated with interaction regions, but the average bulk speed along the whole trajectory was higher (see Table 4 in paper 1). It is possible that these differences between the two Voyagers were related with the data gap in Voyager 1 and/or transient events (e. g.. ejecta) that were detected predominantly only by one spacecraft, however, this point requires further study. The fourth column presents the average and standard deviation of the ratios of thermal pressures, In this case the average values obtained by the two Voyagers were very similar anti higher than the values obtained by Pioneer 1] and Ulysses. Finally, the fifth column presents the average and standard deviation of the ratios of magnetic pressures where again the average values obtained by Voyagers were higher than the vales obtained by Ulysses and Pioneer 11.

'1'o study in more detail the variances in the physical parameters associated with the interaction regions, Figures 5, 6 and 7 show the values of these parameters against heliocentric distance as detected by the three missions. The top panels show the bulk

speeds of the fast and slow streams and the lower panels show the plots of the three pressure ratios associated with every interaction region. In order to make the visual exposure of the plots more intuitive, when the pressure value of the slow stream was higher than the pressure value of the fast stream ($r < 1$) then we 'redefined' the pressure ratio as: r = -- pressure slow stream / pressure fast stream (i. e.. if $r < 1$ then $r = -r^{-1}$).

Figure 5 presents Voyagers observations, '1 'he top panel shows that the bulk speeds of the fast streams causing interaction regions were very variable (see also Figure 8a, b in paper 1). The three lower panels show clearly how the pressure ratios between fast and slow streams also vary continuously and there is not a clear tendency with the heliocentric evolution (at least from 1 to 5 AU). In Voyager 1 observations we studied 15 interaction regions where: about 27% had $r_{dyn.}$ lesser than 1; about 47% had $r_{ther.}$ lesser than 1; and about 47% had $r_{mag.}$ lesser than 1. In Voyager 2 observations wc studied 10 interaction regions where: about 7070 had $r_{dyn.}$ lesser than 1; about 30% had $r_{ther.}$ lesser than 1; and 47'% had $r_{mag.}$ lesser than 1. These remarkable differences between the contemporary measurements by Voyagers 1 and 2 at different heliographic locations. suggest that interaction regions at the ascending phase of the cycle have very irregular shapes and characteristics as a consequence of inhomogeneous solar wind streams.

Figure 6 presents the parameters of the interaction regions detected by Ulysses. The plots show the variations in the patterns of solar wind bulk speeds (see also Figure 8c in paper 1) and the pressure ratios. In Ulysses observations We studied 14 interaction regions where: about 50% had $r_{dyn.}$ and $r_{ther.}$ lesser than 1 (always that $r_{dyn.} < 1$, $r_{ther.} < 1$ in a one-to-one correspondence); and about 64% had $r_{mag.}$ lesser than 1. In

this case we did not find a clear correlation between $r_{mag.}$ and the other two pressure ratios $r_{dyn.}, r_{ther.}$.

Figure 7 shows the parameters of the interaction regions detected by Pioneer 11, The plot of bulk speeds is contrasting compared with Voyager observations, however, the pressure ratios show similar variations. It is interesting to compare Figure 7 with Figures 7 and 8c in paper 1. From about 2.3 to 3.2 AU Pioneer 11 detected a change in the pattern of solar wind speeds and magnetic sector-s, this period coincides with ratios of dynamic pressures lesser than 1 in Figure 7. This shows that the variances in the ratios of pressures arc associated with temporal fluctuations in the pattern of solar wind streams. In Pioneer 11 observations we studied 37 interaction region where: about 49% had $r_{dyn.}$ lesser than 1; about 37% had $r_{ther.}$ lesser than 1; and about 48% had $r_{mag.}$ lesser than 1,

Figure 8 shows the histogram distribution of the bulk speeds of the fast and slow streams associated with interaction regions as detected by the three missions. The left-hancl of Figure 8 shows that the speed distribution of the slow winds was very similar in Voyagers and Pioneer 11, however, Ulysses detected faster slow winds. The right-hand of Figure 8 shows that the distribution of fast winds of the three missions was very different. Voyagers detected the slower fast winds. Ulysses detected a predominantly fast stream around 650 km/s and Pioneer 11 shows a disperse distribution covering from about 400 km/s to about 750 km/s.

4. Conclusions

A summary of the results presented in the previous sections is given next. From the analysis of the geometry of 38 stream interfaces wc found that:

. The interaction regions detected by Voyagers and Pioneer 11 had broad distributions of latitudinal inclinations. In both missions: about 55% of their interaction regions had an absolute latitudinal tilt $|\theta_{si}|$ larger than 100and about 45% of their interaction regions had an absolute latitudinal tilt $|\theta_{si}|$ lesser than 100. On the other hand. the interaction regions detected by Ulysses had very low latitudinal inclinations where about 90% of them had an absolute latitudinal tilt $|\theta_{si}|$ lesser than 5°.

• 'l'he distribution of longitudinal orientations of the interaction regions detected by Voyagers and Ulysses were very similar. In both missions: about 67% of their interaction regions were more azimuthal oriented than the Parker spiral ($\Delta\phi \leq -10°$) and 33% of their interaction regions win-c closely oriented along the Parker spiral ($|\Delta\phi| < 10°$).

. 'The interaction regions detected by Pioneer 11 had a broad distribution of longitudinal orientations where about 50% of them were closely oriented along the Parker spiral (I $\Delta\phi| < 100$), 20% of them were more azimuthal oriented than the Parker spiral ($\Delta\phi \leq -10°$), and 30% of them were more radial oriented than the Parker spiral ($\Delta\phi \geq 10°$).

In paper 1 wc showed that interaction regions can have different wideness at about the same heliocentric distance (Figure 10 in paper 1). The results presented here show that interaction regions can have also different geometry (which might explain the broad distributions of the θ_{B_n}'s of the corotating shocks detected by Ulysses (Figures 6 and 9 in *González-Esparza et* al. [1996])). Some of these results might be associated with solar cycle variations as the latitudinal tilts of the interaction regions detected by Ulysses and Pioneer 11, However, the diversity in the wideness ant] large-scale geometry of stream interfaces seem to be related to fluctuations in the properties of the fast and slow streams causing the interaction regions.

We did not find a clear tendency in the orientation of the stream interfaces to evolve with the heliocentric distance (from 1 to 5 AU). The reason was that the three missions detected several changes in the patterns of solar wind streams affecting the solar wind large-scale dynamics (see paper 1), so the variances in the orientat ions were more so related to these temporal changes than to heliocentric effects.

From the analysis of the physical parameters of the fast and slow streams associated with 75 interaction regions we found that:

- In genera], the bulk speeds of the fast streams behind the interaction regions detected by Voyagers had much lower values than the values detected by Ulysses and Pioneer 11. The three missions detected very different distributions of this parameter.

. The bulk speed distribution of the slow streams preceding the interaction regions were very similar in Voyagers and Pioneer 11 observations, but Ulysses detected faster slow streams.

. As a consequence of the difference in proton density, in about half of the interaction regions detected by the three missions the dynamic pressure of the uncompressed slow stream was higher than the dynamic pressure of the uncompressed fast stream.

. "The three missions detected variances in the ratios of thermal and magnetic pressures between the fast and slow streams associated with interaction regions.

. We fount] many differences in the simultaneous measurements of solar wind dynamics at different heliocentric locations by Voyagers 1 and 2. 'This suggests that during the ascending phase of the solar cycle (and probably at, other phases too) the patterns of solar wind streams arc highly inhomogeneous producing interaction regions with irregular shapes and characteristics.

Contrary to the usual assumption that the fast stream has the higher pressure we have found that the ratio pressures (dynamic, thermal, magnetic) between fast anti slow winds vary continuously. In about half of the cases the slow wind transfers momentum to the fast wind. This variability of the pressure ratios can give us a clue to understand why there are very different interaction regions, why there are variations in the geometry of the interaction regions and what are the limitations in the assumptions of the models of corotating flows.

Acknowledgments. The plasma and magnetic field data for this study were obtained from the National Space Science Data Center at Goddard Space Flight Center. The Pioneer 10 and 11 plasma data are from the experiment of J. Wolfe. The Voyager 1 and 2 plasma data are from the experiment of H. Bridge and J. Belcher. The Voyager 1 and 2 magnetic field data are from the experiment of N. Ness. The Ulysses plasma data are from the experiment of 1). McComas. The Ulysses magnetic field data. are from the experiment of A. Balogh. J.A.G-E. is grateful to the National Research Council for financial support as a Resident Research Associated at JPL. The research at Jet l'repulsion Laboratory, California institute of 'J'ethnology, was supported by the National Aeronautics and Space Administration.

References

Burlaga, L. F., Interplanetary stream interfaces, *J. Geophys. Res., 79, 3717, 1974.*

Burton, M., 13. J. Smith, A. Balogh, R. J. Forsyth, and B. E. Goldstein, Ulysses out-of-ecliptic observations of interplanetary shocks, *Astron. Astrophys. Suppl.* Ser., in press, 1996.

Feldman, W. C.. J. R. Asbridge, S. J. Bame, and J. T. Gosling, Long-term solar variations of selected solar wind properties: Imp 6,7, and 8 results, *J. Geophys. Res.*, 83, 2177-2189. 1978.

Feldman, W. C., J. R. Asbridge, S. J. Bame, and J, T. Gosling, Long-term solar wind electron variations between 1971 and 1978, *J. Geophys. Res., 84,* 7371-7377, 1979.

Gazis, P. R., Long-term enhancements in solar wind speed, *J. Geophys. Res.. 101, 415-424,* 1996.

Gazis, P. R., J. D. Richardson, and K. I. Paularena, Long term periodicity in solar wind velocity during the last three solar cycles, *Geophys. Res. Lett.*, 22, 1165-1168, 1995.

González-Esparza, J. A., A. Balogh, R. J. Forsyth, M. Neugebauer, E. J. Smith. and J. 1,. Phillips, Interplanetary shock waves and large-scale structures: Ulysses' observations in and out of the ecliptic plane, *J. Geophys. Res., 101,* 17057 -17072, 1996.

González-Esparza and E. J. Smith, Solar cycle dependence of the solar wind dynamics: Pioneer, Voyager, and Ulysses from 1 to 5 au, *J. Geophys. Res., 101, in press,* 1996 (Paper 1).

Gosling, J. T'., J. R. Asbridge, S. J. Bame, and W. C. Feldman, Solar wind speed variations: 1962-1974. *J. Geophys. Res.*, 81, 5061, 1976.

Gosling, J. T., J. R. Asbridge, S. J. Bame, and W, C. Feldman, Solar wind stream interfaces, *J. Geophys. Res.,* 83, 1401-1412, 1978.

Gosling, J. T. , S. J. Bame, D. J. McComas, J. L. Phillips, V. J. Pizzo, B.E. Goldstein, and M. Neugebauer, Latitudinal variation of solar wind corotating stream interaction regions: Ulysses, *Geophys.* Res. *Lett.*, 20, 2789-2792, 1993.

Gosling, J. 'l'., W. C. Feldman, D. J. McComas, J. I,. Phillips, V. J. Pizzo, and R. J. Forsyth, Ulysses observations of opposed tilts of solar wind corotating interaction regions in the northern and southern hemispheres, *Geophys. Res. Lett.*, 22, 3333-3336. 1995.

Hoeksema, J. T., The relationship of the large-scale solar field to the interplanetary magnetic field: what will ulysses find?, in *The Sun and the Heliosphere in Three-Dimensions*, edited by R. G. Marsden, pp. 241-254, D. *Reidel*. Norwell. Mass., 1986.

Hu, Y. Q.. Evolution of corotating stream structures in the heliospheric equatorial plane. *J. Geophys. Res.*, *98, 13201-13214.1993.*

Hundhausen, A. J., R. T. Hansen, and S. F. Hansen, Coronal evolution during the sunspot cycle: Coronal holes observed with the Mauna Loa k-coronal neters, *J. Geophys. Res.*, *86, 2079-2094,* 1981.

Mihalov, J. I)., A. Barnes. A. J. Hundhausen, and E. J. Smith. Solar wind and coronal structure near sunspot minimum: Pioneer and smm observat ions from 1985-1987. *J. Geophys. Res.*, *95, 8231-8242, 1990.*

Pizzo, V. J., A three-dimensional model of corotating streams in the solar wind, *J. Geophys. Res.*, *87, 4374-4394,* 1982.

Pizzo, V. J., The evolution of corotating stream fronts near the ecliptic plane in the inner solar system, 2, Three-dimensional tilted-dipole fronts, *J, Geophys. Res.*, *96, 5405-5420,* 1991.

Pizzo, V J., Global, quasi-steady dynamics of the distant solar wind. 1. origin of north-south

flows in the outer heliosphere, *J. Geophys. Res.*, 99, 4173-4183, 1994.

Pizzo, V. J., and J. T. Gosling, 3-I) simulations of high latitude interaction regions: comparation with Ulysses observations, *Geophys. Res. Lett.*, 21, 2063, 1994.

Richardson, J. D., K. I, Paularena, J. W. Belcher, and A. J. Lazarus, Solar wind oscillations with a 1.3-year period, *Geophys. Res. Lett.*, *21,1559,* 1994.

Riley, P., J. T. Gosling, I,. A. Weiss, and V. J. Pizzo, The tilts of corotating interaction] regions at midheliographic latitudes, *J. Geophys. Res., 101, in press,* 1 996.

Siscoe, G. I,., Structure and orientation of solar-wind interaction fronts: pioneer 6, *J. Geophys. Res.*, 77, 27, 1972.

Siscoe, G. I,., Three-dimensional aspects of interplanetary shock waves. *J. Geophys.* lies., *81,* 6235, 1976.

Siscoe, G. L., B. Goldstein, and A. J. Lazarus, An east-west asymmetry in the solar wind velocity. *J. Geophys. Res., 74,* 1759, 1969.

Smith, E. J., The heliospheric current sheet and modulation of galactic cosmic rays, *J. Geophys. Res., 95,* 18731-] 8743, 1990.

Zhao, X., and A. J. Hundhausen, Organization of solar Wind plasma properties in a tilted, heliomagnetic system, *J. Geophys. Res., 86,* 5423, 1981.

This manuscript was prepared with the AGU LaTeX macros v3.0.

Figure 1. Example of an interaction region detected by Pioneer 11 containing a well-defined stream interface. The top panel shows the two polar angles of solar wind velocity in heliospheric coordinates (ϕ longitudinal, θ latitudinal). The mid panel shows the discontinuity in proton density and proton temperature. The bottom panel shows the solar wind radial velocity and the magnetic field magnitude. The solar wind plasma data (1 hour averages) was obtained from the NSSDC.

Figure 2. Latitudinal orientation of the stream interfaces θ_{si} detected by the four spacecraft against heliocentric distance. Where $\theta_{si} > 0°$ implies that the front Of the interaction region was pointing northern, $\theta_{si} \approx 0°$ implies that the interaction region was orthogonal to the ecliptic plane, and $\theta_{si} <$ O" implies that the front of the interaction region was pointing southern.

Figure 3. Distribution histograms of the latitudinal orientation of the interfaces θ_{si} as detected by the three missions. The three distribution show clear differences that might be related with the solar cycle. Ulysses low θ_{si}s might be related to interaction regions caused by equatorial coronal holes; Pioneer 11 high θ_{si}s might be associated with the tilt solar geometry at the descending phase of the cycle.

Figure 4. Distribution histograms of the longitudinal orientation of the stream interfaces with respect to the Parker spiral $\Delta\phi$ as detected by the three missions. Where $\Delta\phi \approx 0°$ indicates that the interface was oriented along the Parker spiral, $\Delta\phi < 0°$ indicates that the interface was more azimuthal the Parker spiral, and $\Delta\phi > 0$" indicates that the interface was oriented more radial than the Parker spiral. Voyagers and Ulysses results are statistically similar. Pioneer 11 shows a more diverse distribution.

Figure 5. Physical parameters (against heliocentric distance) associated with the interaction regions detected by Voyagers 1 and 2. The top panel shows the bulk speeds of the fast and slow streams causing interaction regions. Below, the pressure ratios between the fast and slow streams (dynamic $r_{dyn.}$, thermal $r_{ther.}$, and magnetic $r_{mag.}$). In order to facilitate the visual comparison, when the pressure of the slow stream was higher than the pressure of the fast stream ($r < 1$) then we redefined the ratio as $r =$ -- (pressure slow wind/ pressure fast wind). The plots show continual variations in the properties of the fast and slow winds causing interaction regions.

Figure 6. Physical parameters associated with the interaction regions detected by Ulysses. The plots are presented with the same format of Figure 5.

Figure 7. Physical parameters associated with the interaction regions detected by Pioneer 11. The plots are presented with tile same format of Figure 5. The variations detected from about 2.5 to 3.2 AU were associated with changes in the pattern of solar wind streams and magnetic sectors (Figures 7 and 8e in paper 1).

Figure 8. Bulk speed distribution histograms of the (a) slow and (b) fast solar wind streams causing interaction regions as detected by the three missions. The distribution of slow winds was very similar in Voyagers and Pioneer 11 observations, but Ulysses detected faster slow winds. The distributions of fast winds were very different in the three missions.

Table 1. Comparison of physical parameters of the fast and slow solar wind streams causing interaction regions as observed by the four spacecraft,.

Spacecraft	No.	$\bar{V}_F$	$\bar{V}_S$	$\bar{r}_{dyn.}$	$\bar{r}_{ther.}$	$\bar{r}_{mag.}$
Voyager 1	15	495 km/s	371 km/s	1.6 ± 1.1	2.53. 2.8	2.0 ± 2.0
Voyager 2	10	472 km/s	342 km/s	0.9:1" 0.8	2.6 ± 2.6	1.7 ± 1.6
Ulysses	14	574 km/s	*412* km/s	1.13 .0.9	1.5 ± 1.6	1.2 ± 1.4
Pioneer 11	36	592 km/s	386 km/s	1.15 0.8	1.8 ± 1.8	1.6 ± 1.6

† Second column: number of interaction regions analyzed for each spacecraft. Third column: average of bulk speed of the fast, streams behind the interaction regions. Fourth column: average of bulk speed of the slow streams preceding the interaction] regions. Fifth column: average and standard deviation of the ratios of dynamic pressures between fast and slow streams. Sixth column: average and standard deviation of the ratios of thermal pressures. Seventh column: average and standard deviation of the ratios of magnetic pressures.

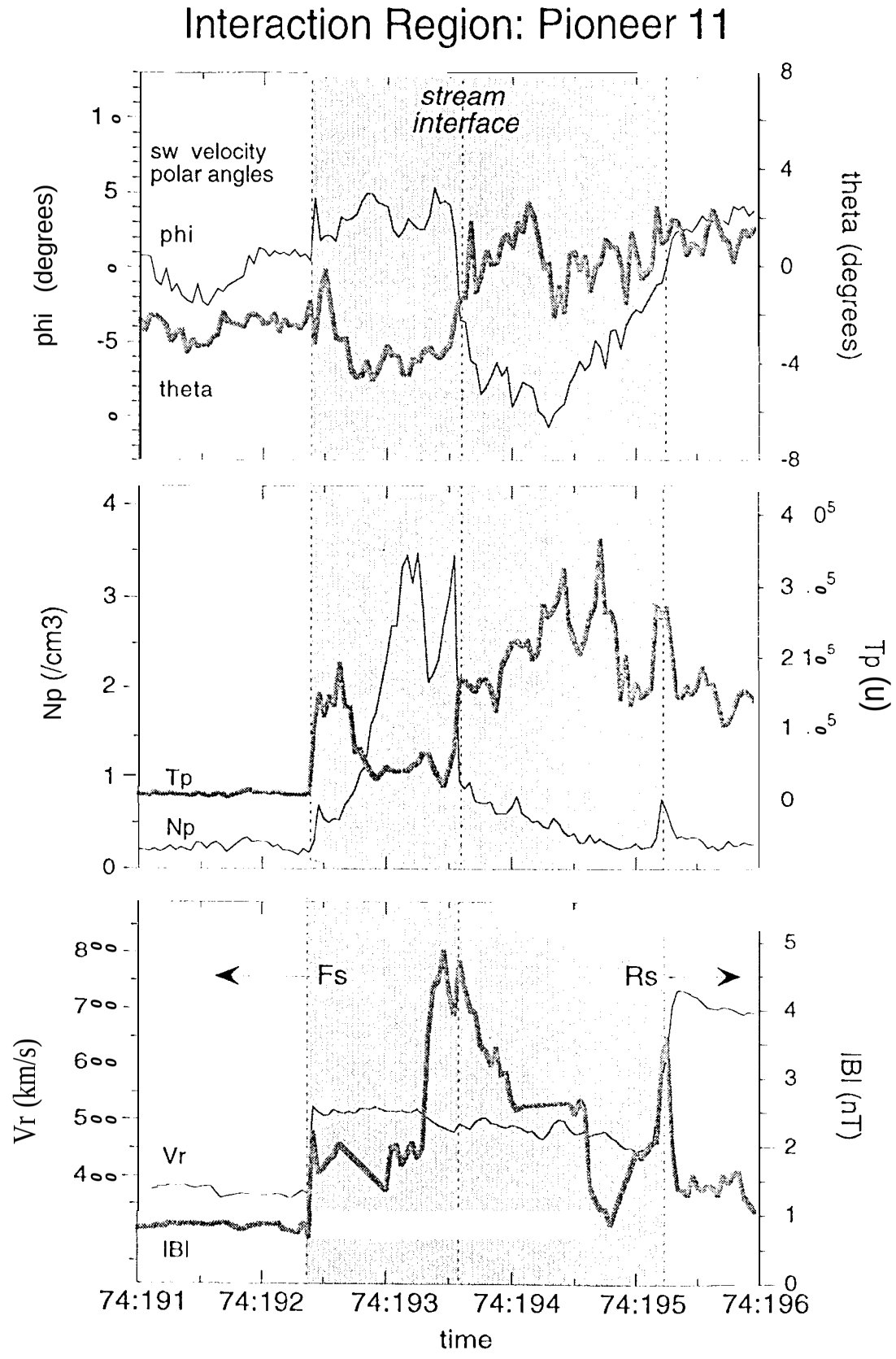
Interaction Region: Pioneer 11
stream interface
sw velocity polar angles
phi
theta
phi (degrees)
theta (degrees)
Np (/cm3)
Tp (u)
Tp
Np
Fs
Rs
Vr (km/s)
IBI (nT)
Vr
IBI
74:191
74:192
74:193
74:194
74:195
74:196
time

Figure 1

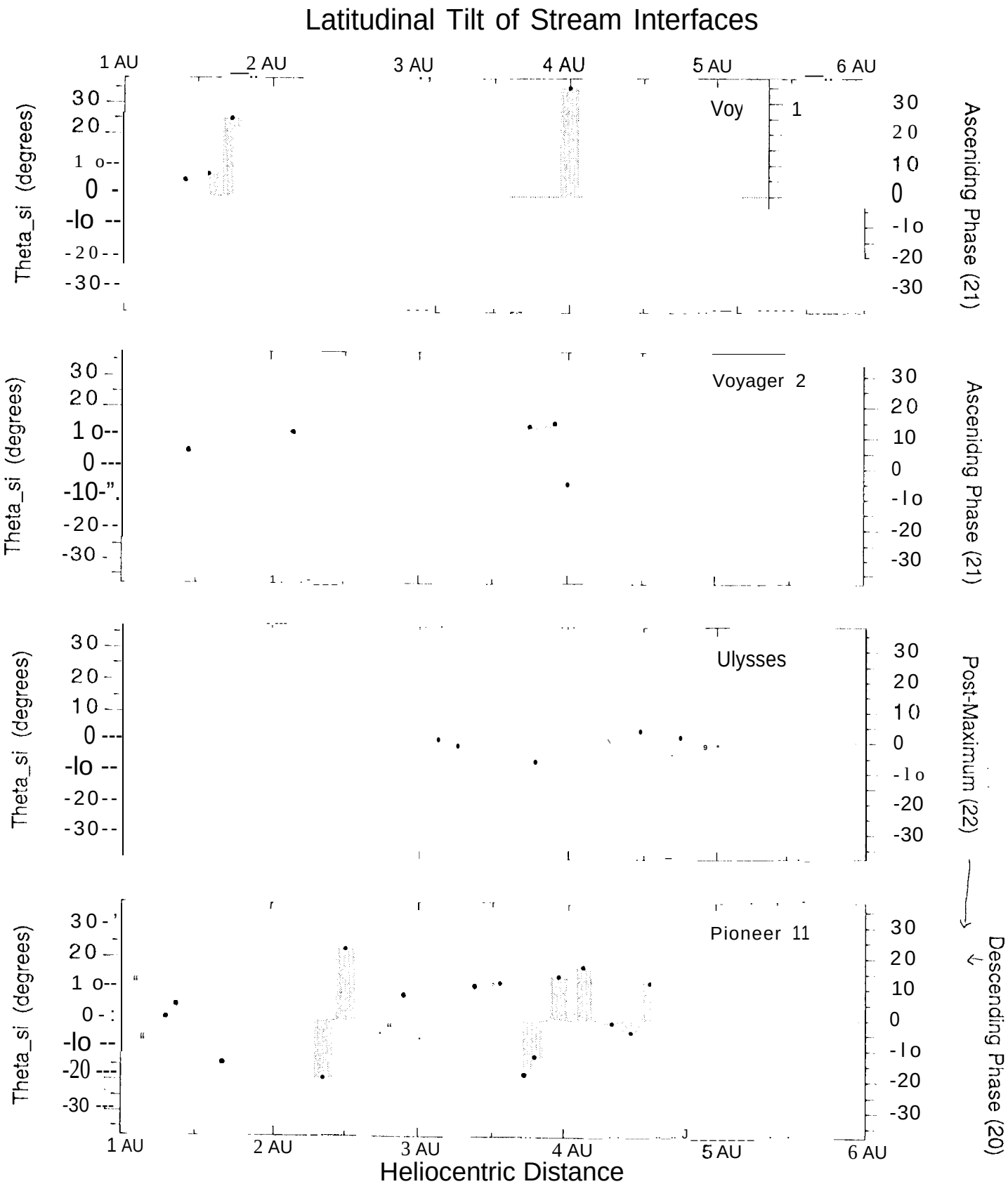
Latitudinal Tilt of Stream Interfaces
1 AU
2 AU
3 AU
4 AU
5 AU
6 AU
Theta_si (degrees)
Voy 1
Voyager 2
Ulysses
Pioneer 11
Ascending Phase (21)
Post-Maximum (22)
Descending Phase (20)
Heliocentric Distance

Figure 2

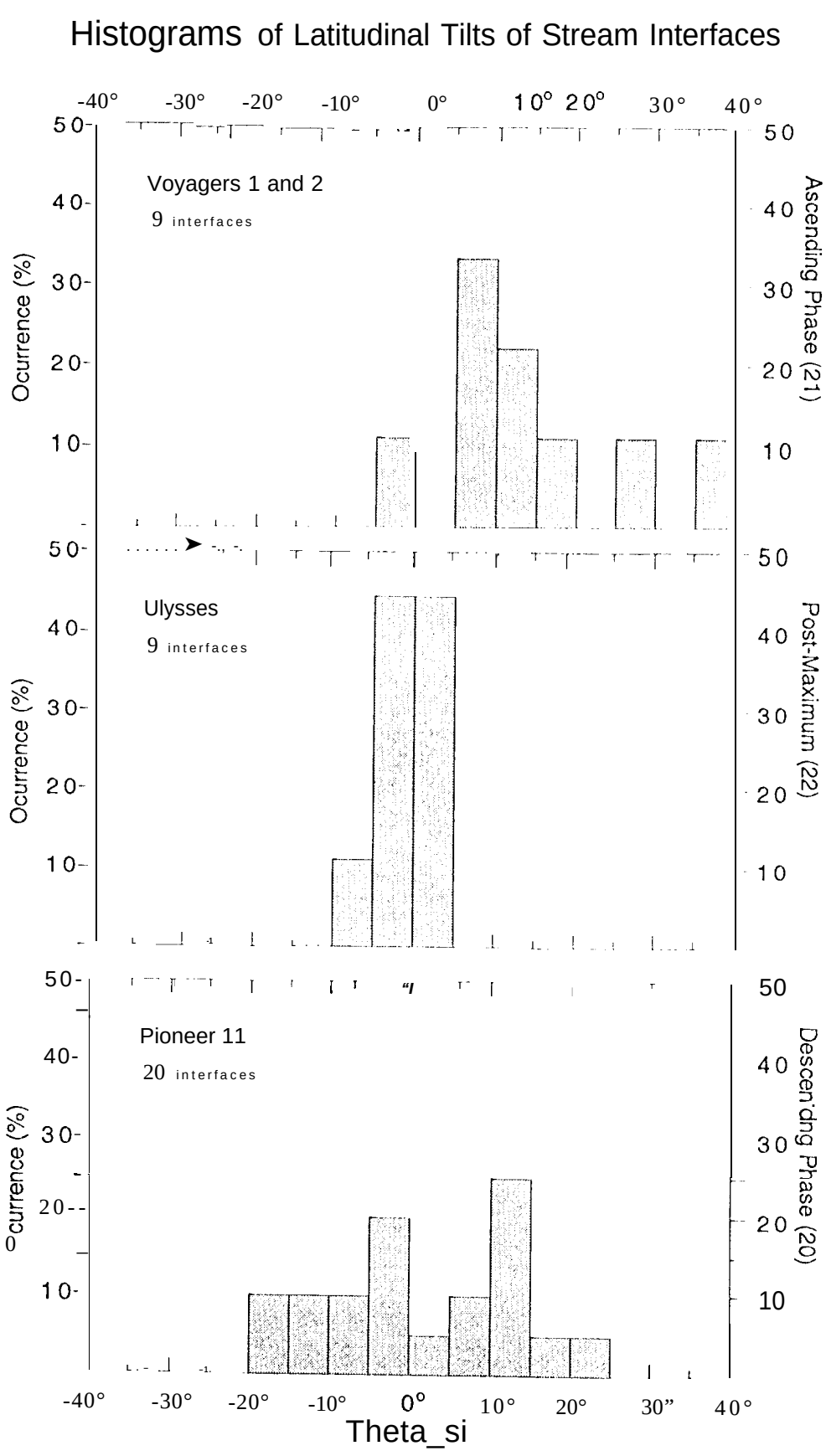
Histograms of Latitudinal Tilts of Stream Interfaces
-40°
-30°
-20°
-10°
0°
10°
20°
30°
40°
Voyagers 1 and 2
9 interfaces
Ocurrence (%)
Ascending Phase (21)
Ulysses
9 interfaces
Post-Maximum (22)
Pioneer 11
20 interfaces
Descending Phase (20)
Theta_si

Figure 3

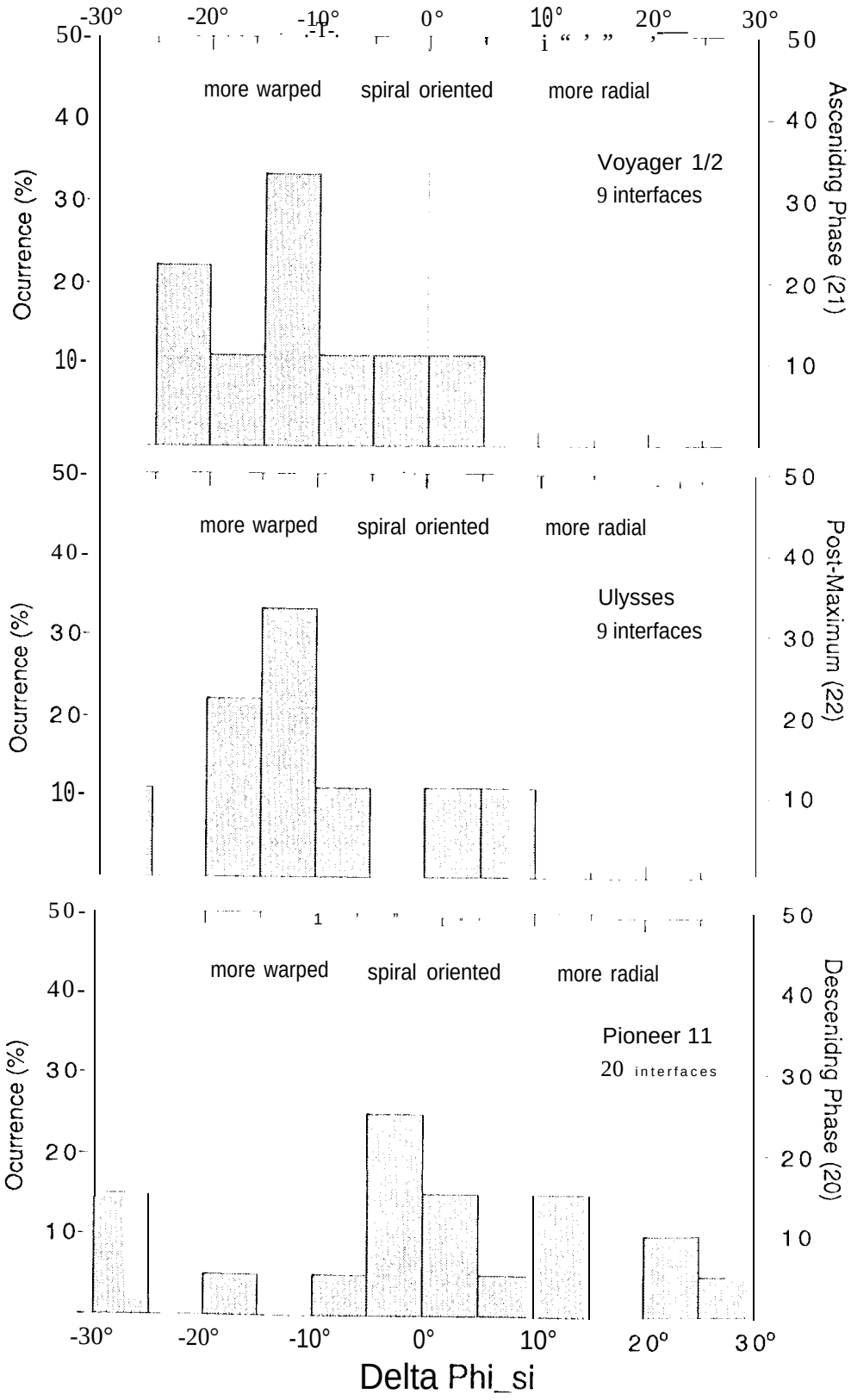
Histograms of Longitudinal Spiral Orientation
-30°
-20°
-10°
0°
10°
20°
30°
more warped
spiral oriented
more radial
Voyager 1/2
9 interfaces
Ocurrence (%)
Asceniding Phase (21)
Ulysses
9 interfaces
Post-Maximum (22)
Pioneer 11
20 interfaces
Descending Phase (20)
Delta Phi_si

Figure 4

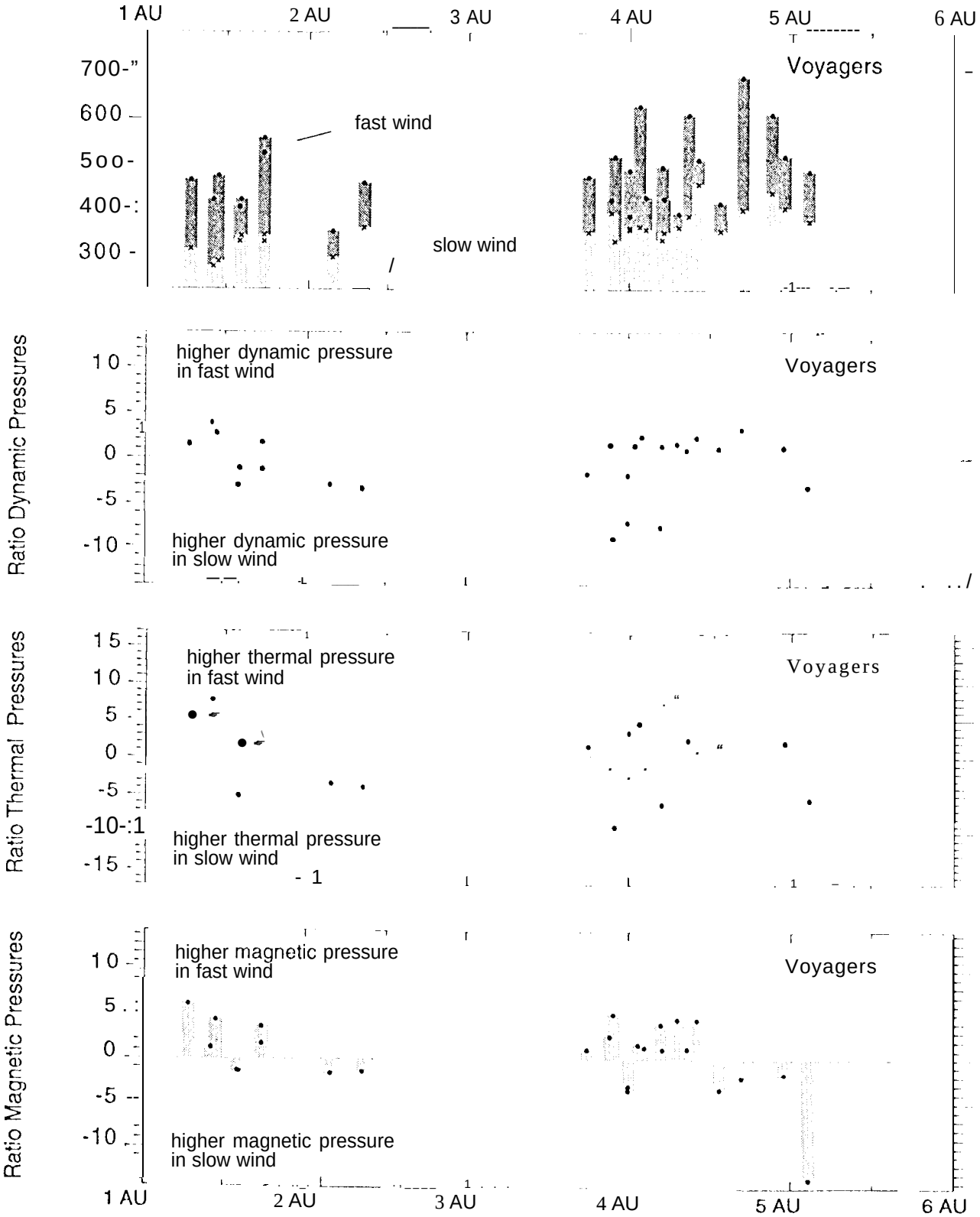
1 AU
2 AU
3 AU
4 AU
5 AU
6 AU
700
600
500
400
300
fast wind
slow wind
Voyagers
Ratio Dynamic Pressures
10
5
0
-5
-10
higher dynamic pressure in fast wind
higher dynamic pressure in slow wind
Voyagers
Ratio Thermal Pressures
15
10
5
0
-5
-10
-15
higher thermal pressure in fast wind
higher thermal pressure in slow wind
Voyagers
Ratio Magnetic Pressures
10
5
0
-5
-10
higher magnetic pressure in fast wind
higher magnetic pressure in slow wind
Voyagers
1 AU
2 AU
3 AU
4 AU
5 AU
6 AU

Figure 5

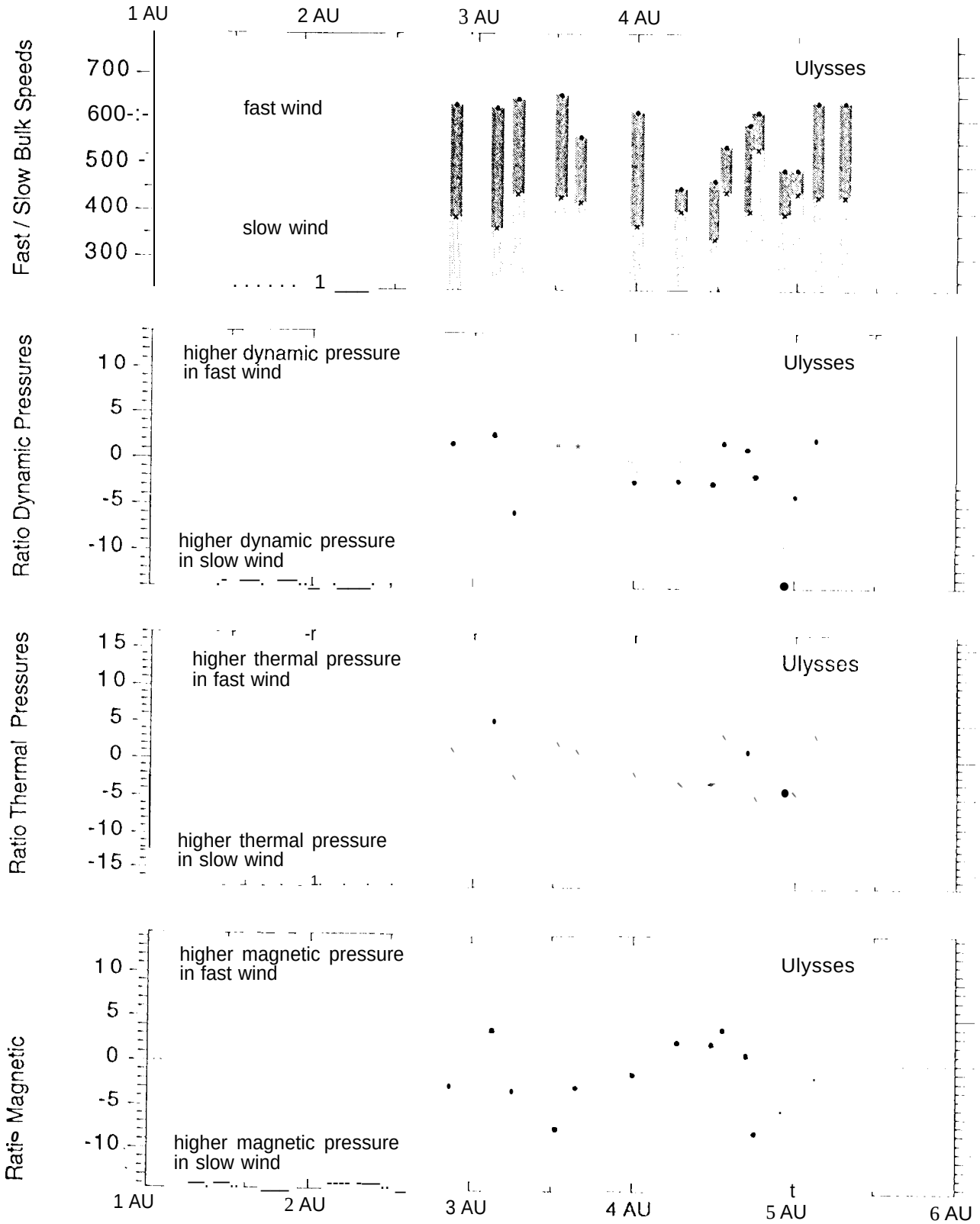
1 AU
2 AU
3 AU
4 AU
Fast / Slow Bulk Speeds
700
600
500
400
300
fast wind
slow wind
Ulysses
Ratio Dynamic Pressures
10
5
0
-5
-10
higher dynamic pressure in fast wind
higher dynamic pressure in slow wind
Ulysses
Ratio Thermal Pressures
15
10
5
0
-5
-10
-15
higher thermal pressure in fast wind
higher thermal pressure in slow wind
Ulysses
Ratio Magnetic
10
5
0
-5
-10
higher magnetic pressure in fast wind
higher magnetic pressure in slow wind
Ulysses
1 AU
2 AU
3 AU
4 AU
5 AU
6 AU
t

Figure 6

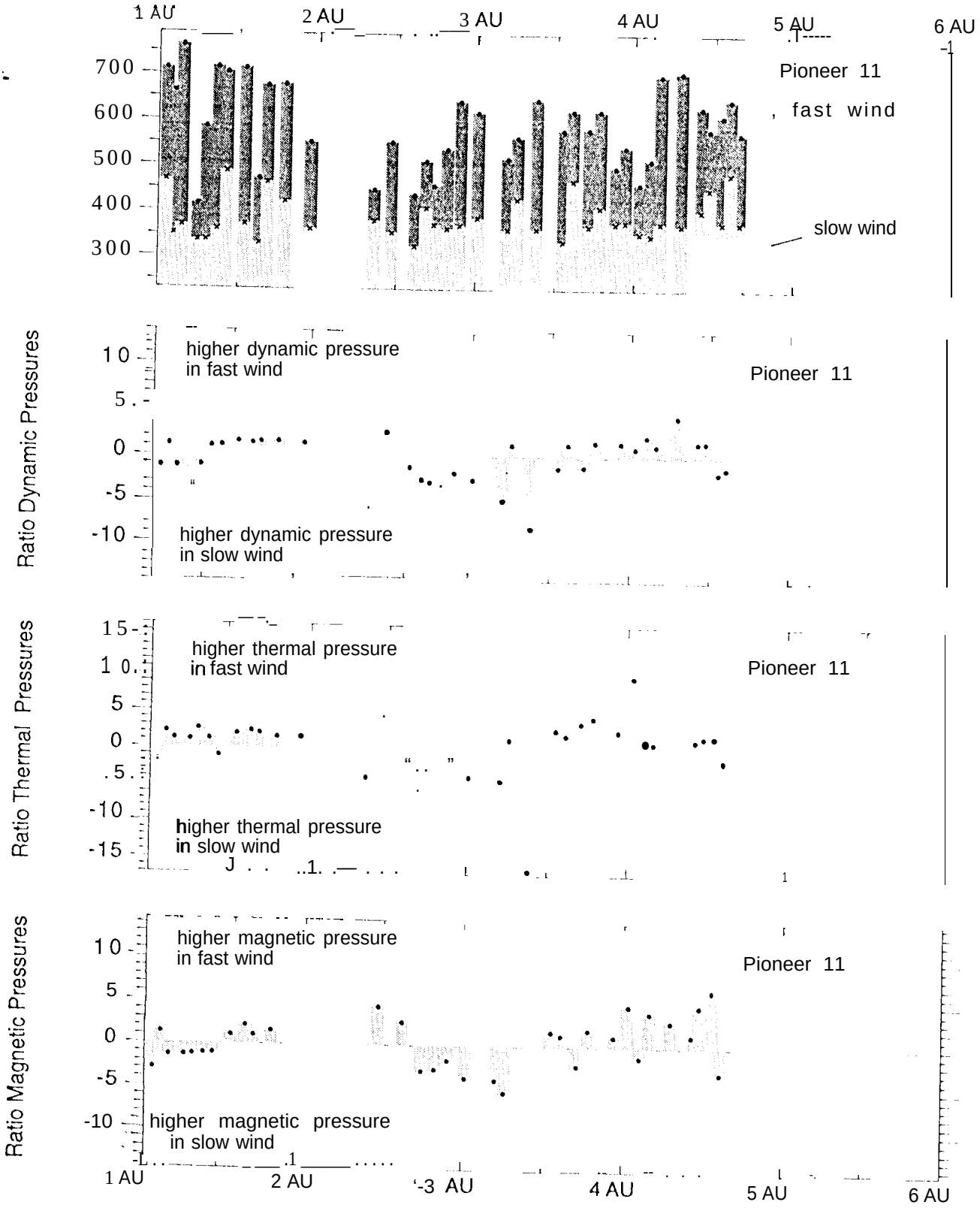
1 AU
2 AU
3 AU
4 AU
5 AU
6 AU
700
600
500
400
300
Pioneer 11
, fast wind
slow wind
Ratio Dynamic Pressures
10
5
0
-5
-10
higher dynamic pressure
in fast wind
Pioneer 11
higher dynamic pressure
in slow wind
Ratio Thermal Pressures
15
10
5
0
-10
-15
higher thermal pressure
in fast wind
Pioneer 11
higher thermal pressure
in slow wind
Ratio Magnetic Pressures
10
5
0
-5
-10
higher magnetic pressure
in fast wind
Pioneer 11
higher magnetic pressure
in slow wind
1 AU
2 AU
3 AU
4 AU
5 AU
6 AU

Figure 7

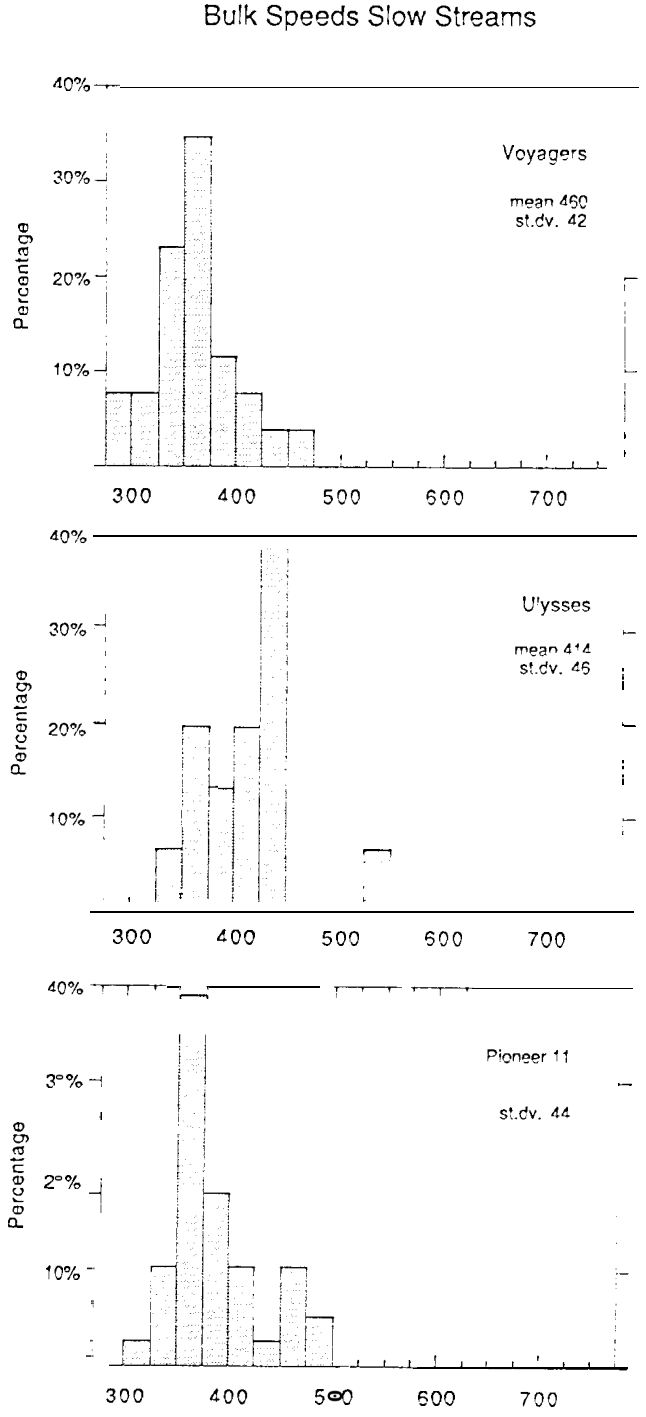
Bulk Speeds Slow Streams
Voyagers
mean 460
st.dv. 42
U'ysses
mean 414
st.dv. 46
Pioneer 11
st.dv. 44
Percentage
40%
30%
20%
10%
300
400
500
600
700

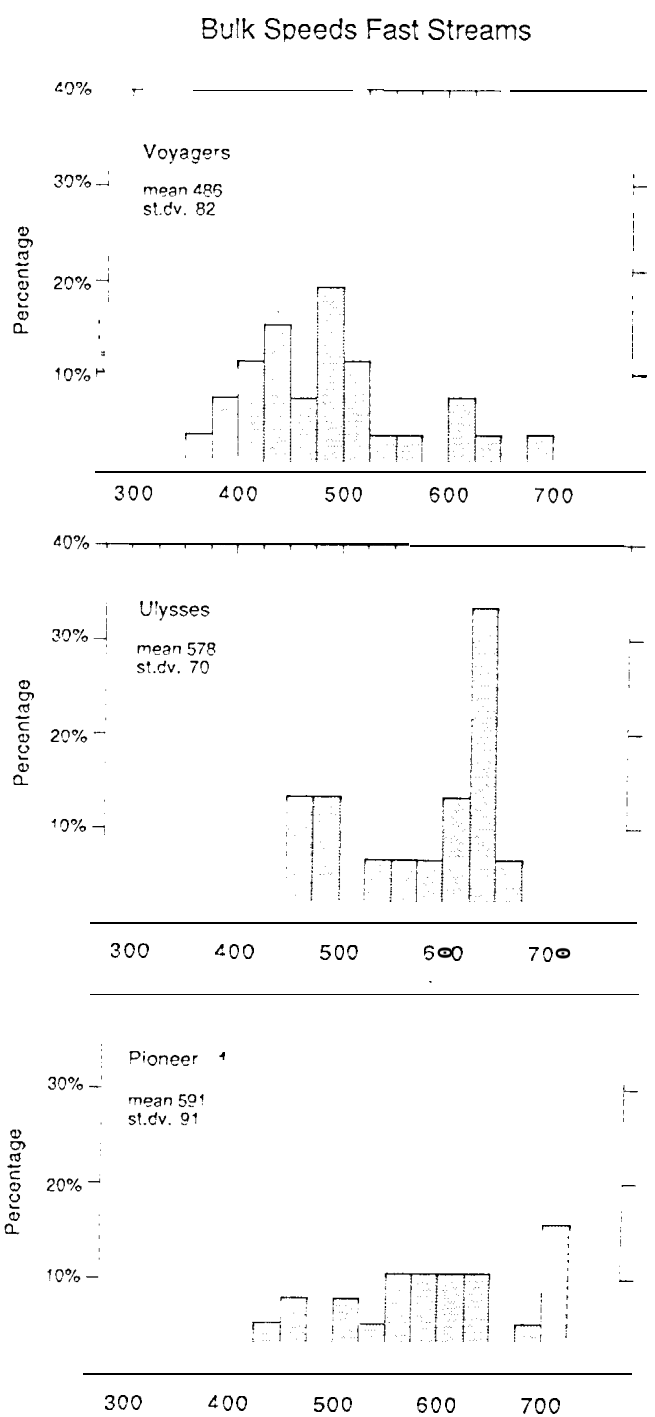
Bulk Speeds Fast Streams
Voyagers
mean 486
st.dv. 82
U'ysses
mean 578
st.dv. 70
Pioneer
mean 591
st.dv. 91
Percentage
40%
30%
20%
10%
300
400
500
600
700

Figure 8